Title	Treatment with functionalized designer self-assembling peptide hydrogels promotes healing of experimental periodontal defects
Author(s) Alternative	Matsugami, D; Murakami, T; Yoshida, W; Imamura, K; Bizenjima, T; Seshima, F; Saito, A
Journal	Journal of periodontal research, 56(1): 162-172
URL	http://hdl.handle.net/10130/5784
Right	This is the peer reviewed version of the following article: J Periodontal Res. 2021 Jan;56(1):162-172, which has been published in final form at https://doi.org/10.1111/jre.12807. This article may be used for non-commercial purposes in accordance with Wiley Terms and Conditions for Use of Self-Archived Versions. This article may not be enhanced, enriched or otherwise transformed into a derivative work, without express permission from Wiley or by statutory rights under applicable legislation. Copyright notices must not be removed, obscured or modified. The article must be linked to Wiley's version of record on Wiley Online Library and any embedding, framing or otherwise making available the article or pages thereof by third parties from platforms, services and websites other than Wiley Online Library must be prohibited.
Description	

Original Article

Revised: JRE-06-20-5782

Treatment with functionalized designer self-assembling peptide hydrogels promotes healing of experimental periodontal defects

D. Matsugami[1,3], T. Murakami[1], W. Yoshida[1], K. Imamura[1,3], T. Bizenjima[2], F. Seshima[1], A. Saito[1,3]

[1]Department of Periodontology, Tokyo Dental College, Tokyo, Japan

[2]Tokyo Dental College Chiba Dental Center, Chiba, Japan

[3]Oral Health Science Center, Tokyo Dental College, Tokyo, Japan

Correspondence author: Atsushi Saito, DDS, PhD

Professor and Chair, Department of Periodontology, Tokyo Dental College

2-9-18 Kanda-Misakicho, Chiyoda-ku, Tokyo 101-0061, Japan

Phone: +81-3-6380-9171 Fax: +81-3-6380-9172

E-mail: atsaito@tdc.ac.jp

Running Title: Designer SAP hydrogels and defect healing

Key words: self-assembling peptide, functionalized motif, cell proliferation, periodontal defect

Abstract

Background/Objectives: It has been reported that self-assembling peptide (SAP) hydrogels with functionalized motifs enhance proliferation and migration of host cells. How these designer SAP hydrogels perform in the treatment of periodontal defects remains unknown. This study aimed to test the performance of local application of designer self-assembling peptide (SAP) hydrogels with two different functionalized motifs in the treatment of experimental periodontal defects.

Materials and Methods: *In vitro*, viability/proliferation of rat periodontal ligament-derived cells (PDLCs) cultured on an SAP hydrogel RADA16 and RADA16 with functionalized motifs, PRG (integrin binding sequence) and PDS (laminin cell adhesion motif), was assessed. Cell morphology was analyzed by scanning electron microscopy (SEM) and confocal laser scanning microscopy (CLSM). *In vivo*, standardized periodontal defects were made mesially in the maxillary first molars of Wistar rats. Defects received RADA16, PRG, PDS or left unfilled. At 2 or 4 weeks postoperatively, healing was assessed by microcomputed tomography, histological and immunohistochemical methods.

Results: Viability/proliferation of PDLCs was significantly greater on PRG than on RADA16 or PDS at 72 hours. rPDLCs in the PRG group showed enhanced elongations and cell protrusions. *In vivo*, at 4 weeks, bone volume fractions in the PRG and PDS groups were significantly greater than the RADA16 group. Histologically, bone formation was more clearly observed in the PRG and PDS groups compared with the RADA16 group. At 4 weeks, epithelial down-growth in the hydrogel groups was significantly reduced compared to the Unfilled group. In Azan-Mallory staining, PDL-like bundles ran in oblique direction in the hydrogel groups. At 2 weeks, in the area near

the root, proliferating cell nuclear antigen (PCNA) -positive cells were detected significantly more in the PRG group than other groups. At 4 weeks, in the middle part of PDL, a significantly greater level of vascular endothelial growth factor (VEGF) -positive cells and α-SMA-positive blood vessels were observed in the PRG group than in other groups.

Conclusion: The results indicate that local application of the functionalized designer SAP hydrogels, especially PRG, promotes periodontal healing by increasing cell proliferation and angiogenesis.

1 Introduction

Among the essential factors for periodontal tissue engineering, scaffolds serve as the template structure for tissue to be regenerated.[1,2] It is desirable for a scaffold material to be osteoconductive and bioresorbable, and to provide an appropriate environment for periodontal regeneration.[3]

Biomimetic matrices are preferred in tissue regeneration because natural materials have risks of infection.[4,5] Self-assembling peptides (SAPs), composed of essential amino acids, possess properties close to those of native extracellular matrix (ECM).[6-8] SAP hydrogels provide a three-dimensional (3-D) environment that fosters proliferation and migration of many types of cells.[9-10] They have been shown not to elicit immunogenic or inflammatory responses.[11-13] An SAP hydrogel, RADA16 has been proposed as a scaffold because it has unique 3-D structure.[6,14] In pre-clinical models, bone regeneration was achieved by using RADA16.[15,16] We previously reported that the local application of RADA16 alone promoted periodontal healing in a rat model.[17]

Cell adhesion is a critical initial step in interaction between cells and materials.[18] Arginyl-glycyl-aspartic acid (RGD), an important binding sequence for cell recognition and attachment, specifically works with integrin.[19,20] It has been reported that RGD containing peptide enhances cell attachment, proliferation and osteoblast differentiation and mineralization.[21,22,23] Laminin is a family of ECM proteins localized primarily in the basement membranes which regulate cell adhesion functions.[24] It has a cell adhesion active site (YIGSR: Tyr-Ile-Gly-Ser-Arg),[25] which changes its structure in various ways, such as polymers and multimers, and is expected to be a functional polymer.[26]

YIGSR peptide has been shown to promote synthesis of type I collagen.[27] In relation to periodontal tissue, previous studies reported that peptides with RGD or laminin cell adhesion motifs promoted activities of periodontal ligament (PDL) fibroblasts.[28-30] RADA16 can be tailored for biological applications by attaching bioactive motifs.[31]

Given these backgrounds, we took interest in two functionalized peptides; PRG, a RADA16 with direct coupling to 2-unit RGD and PDS, with laminin cell adhesion motif.[19] They have been shown to promote cell proliferation, migration, and production of collagen in PDL fibroblasts culture.[19] Preosteoblasts grown on PRG showed high alkaline phosphatase activity and enhanced proliferation and osteogenic differentiation.[32] However, information is limited on the effects of RADA16 with cell adhesion motifs on periodontal healing. We hypothesized that enhanced periodontal regeneration may be achieved by the application of PRG or PDS.

This study aimed to evaluate the effects of SAP nanofiber hydrogels, functionalized with two different peptide motifs, on periodontal defect healing *in vivo*.

2 Materials and Methods

2.1 SAP hydrogels

RADA16 [Ac-$(RADA)_4$-NH_2] (PuraMatrix^{TM}; 3D Matrix, Tokyo, Japan), RADA16 with 2-unit RGD binding sequence [PRG; Ac-$(RADA)_4$-GPRGDSGYRGDS-NH_2] and RADA16 with laminin cell adhesion motif [PDS; Ac-$(RADA)_4$-GGSDPGYIGSR-NH_2] were used as 2.5% hydrogels.

2.2 Scanning electron microscopy

Microstructures of the hydrogels were assessed using scanning electron microscopy (SEM). After two washes with phosphate buffered saline (PBS, PH 7.4), samples of the 2.5% RADA16, PRG and PDS were dehydrated in ethanol. After drying to the critical point of t-butyl alcohol, the samples were coated with Au-Pd using a sputter coater (SC500A; Bio-Rad, Hercules, CA, USA). The samples were then observed with a scanning electron microscope (SU6600; Hitachi, Tokyo, Japan).

Measurement of pore sizes and fiber diameters from the randomly sampled sites in the SEM images was carried out using the calibrated scale in the SEM system and Image J (ver. 1.53c, http://rsb.info.nih.gov/ij).

2.3 Animals

Male Wistar rats (*in vitro* experiments: 4 weeks old; *in vivo*: 10 weeks old) were used (Sankyo Labo Service, Tokyo, Japan). The study was performed in compliance with the ARRIVE guidelines (https://www.nc3rs.org.uk/arrive-guidelines) and the Treatment of Experimental Animals at Tokyo Dental College (approval number 192202).

2.4 Cell proliferation/viability assay

PDL-derived cells (rPDLCs) were obtained from incisors of Wistar rats by the method of Inoue et al.[33] WST-1 assay (Takara Bio, Otsu, Japan) was used to evaluate cell viability/proliferation on RADA16, PRG and PDS as described previously.[34] Briefly, the explants were incubated in α-minimal essential medium (MEM, Gibco Invitrogen, Carlsbad, CA, USA) supplemented with heat-inactivated 10% fetal bovine serum and antimicrobials at 37°C in 5% CO_2 in air. The medium was changed every 48 h until cells had outgrown from the explants and reached near confluency. Cells at the 2nd and 3rd passages were used for the following in vitro experiments. An aliquot (50 μl) of pre-treated hydrogels was added to each well of a 96-well plate. Then, 100 μl MEM was gently added, and incubated for 60 min. Three quarters of the medium volume was replaced with fresh medium, followed by incubation for 30 min. rPDLCs (1 x 10^3) were then seeded onto the hydrogel. At predetermined time points, 10 μl premixed WST-1 reagent (Takara Bio, Otsu, Japan) was added to each well and incubated for 2 h to allow color development. The resulting supernatants were then analysed for absorbance at 450 nm.

2.5 Confocal laser scanning microscopy (CLSM)

rPDLCs were seeded in hydrogels at a density of 2 x 10^5 cells on 24-well culture plates. After incubation for 3 days, the cells on the gel were washed twice with PBS, and fixed with 4% paraformaldehyde for 20 minutes and permeabilized with 0.1% Triton X-100 for 5 minutes at room temperature. Incubation with 3% bovine serum albumin (BSA) for 60 minutes at room temperature prevented non-specific reactions. Alexa Fluor-488

Phalloidin (diluted 1:100) (Life Technologies, Carlsbad, CA, USA) was used to stain F-actin and 4-6-diamino-2-phenylindole (DAPI) (diluted 1:1,000) (Thermo Scientific, Pittsburgh, PA, USA) was used for nuclear staining and incubated for 30 minutes at room temperature. The cells were then examined and photographed using a confocal laser scanning microscope (LSM 880, Carl Zeiss, Oberkochen, Germany).

2.6 Experimental model and surgical procedures

The animals were allocated to the following 4 subgroups: 1) Unfilled (n=10), 2) RADA16 (n=10), 3) PRG (n=10), and 4) PDS (n=10). Under general and local anesthesia, standardized bilateral periodontal defects (2 x 2 x 1.7 mm) were surgically created mesially of the maxillary first molars (M1) according to the method of Bizenjima et al.[35] (Figure S1a-g). The M1 root was denuded of its PDL, cementum and superficial dentin. After rinsing with sterile saline and drying, the defects received 50 µl of 2.5% RADA16, PRG, PDS or left unfilled. Resorbable sutures were used to close the flaps. Acetaminophen was given to control pain. After surgery, sacrifice was performed at 2 or 4 weeks (Figure S1h).

2.7 Microcomputed tomography analysis

At each time point, cardiovascular perfusion was performed after the animals were deeply anesthetized. Maxillae were retrieved, and the healing in the surgical defect was evaluated by microcomputed tomography (R-mCT; Rigaku, Tokyo), according to the method of Takeuchi et al.[17] Image data acquired by micro-CT were analyzed using 3-D reconstruction software (TRI/3D-BON; Ratoc System Engineering, Tokyo) by the method of Bizenjima et al.[35]

2.8 Histological and histomorphometric analyses

The maxillae were split along the palatal median line. After fixation in buffered 4% paraformaldehyde for 24 h, samples were decalcified in 10% ethylenediaminetetraacetic acid disodium salt (EDTA-2Na, pH 7.0) (Muto Pure Chemicals, Tokyo, Japan) at 4°C for 3 weeks and then embedded in paraffin. Mesio-distal sections (thickness 5 μm) were cut with a microtome (Hyrax M25, Carl Zeiss, Jena, Germany). From each specimen, five to ten sections representing the central portion of the root in the defect were stained with hematoxylin-eosin for histological and histomorphometric analyses. Azan–Mallory staining was applied to some sections. The following measurements were made using a software (Axio Vision 4.7; Carl Zeiss Japan) as described previously[35]: 1) root length, 2) length of the junctional epithelium, and 3) the distance between cemento-enamel junction and the defect bottom.

On the root planed surface of M1, the angulation of PDL-like bundles was assessed by Image J software.[36]

2.9 Immunohistochemistry

Paraffin sections were deparaffinized with xylol and incubated in 3% hydrogen peroxide with methanol for 30 min at room temperature. For antigen retrieval, the sections were treated with microwave heating for 3 min. After washing with PBS, sections were incubated with 3% bovine serum albumin for 30 min to block nonspecific binding. Proliferating cell nuclear antigen (PCNA) was detected by as follows: sections were treated with mouse anti-PCNA primary antibody (dil.1:100; PC-10, DAKO, Carpinteria, CA) for 12 h at 4°C, followed by exposure to the HRP-conjugated antibody

(Histofine® Simple Stain Max PO (M), Nichirei, Tokyo) for 60 min at room temperature. After rinsing, they were incubated with diaminobenzidine and counterstained with hematoxylin. Detection of vascular endothelial growth factor (VEGF) was performed using anti-VEGF monoclonal antibody (dil. 1:50; Abcam, Tokyo).

For detection of α-smooth muscle actin (SMA), anti-α-SMA monoclonal antibodies (dil. 1:100; Abcam) were used.

For the analysis of PCNA- or VEGF-positive cells, a field of connective tissue was randomly sampled in each section and submitted to quantification as described previously.[35,37] Each treated site was compartmentalized into three areas to count PCNA- or VEGF-positive cells. The percentage of α-SMA-positive blood vessels to that of total blood vessels was also calculated.

The micro-CT, histomorphometric and immunohistochemical data were evaluated by one examiner who was blinded to the experimental grouping and confirmed by a second independent examiner.

2.10 Statistical analysis

Sample size was estimated by an analysis based on a 90% power with a 0.05 two-sided significance level, given a relevant difference in bone volume between groups of 10.5% (as measured by micro-CT) and a standard deviation of 7% [35], using a software package (StatMate 2, GraphPad Software, San Diego, CA). According to the determination, a sample size of 10 (defect site) in each group was needed. Inter-group comparisons were undertaken using analysis of variance (ANOVA) with Tukey post hoc test (Prism 7.05, GraphPad Software). A *P*-value less than 0.05 was considered statistically significant.

3 Results

3.1 SEM observation of the hydrogel structure

All hydrogels showed fibrous mesh structure with nanopores (pore sizes; 5 – 200 μm) (Figure S2). Surface architecture of nanofibers in RADA16 and PDS was similar, but that of PRG appeared to be different: smoother and finer fiber structure was observed. Fiber diameter of PRG (79.9 ± 5.7 nm) were significantly smaller compared with RADA16 (170.1 ± 13.0 nm) or PDS (133.6 ± 13.3 nm) ($P < .001$).

3.2 Effects of designer SAP hydrogels on cell viability/proliferation

rPDLCs in the PRG group showed significantly higher viability/proliferation than the RADA16 group ($P < .05$) (Figure 1). There was a rapid increase in viability/proliferation in the PRG group from 48 hours, and the value at 72 hours was significantly greater compared with PDS group ($P < .01$).

Morphology of rPDLCs cultured on the hydrogels were observed by SEM (Figure S3). At 72 hours, rPDLCs on RADA16 appeared roundish. In contrast, the cells on the hydrogels with functionalized motif, especially PRG, were elongated and extended pseudopodal projections.

3.3 CLSM analysis

At 72 hours, compared to RADA16 group, rPDLCs in the PRG and PDS groups appeared to be elongated and showed cell protrusions (Figure 2).

3.4 Micro-CT analysis of defect healing

In general, defect healing progressed normally. Sagittal slice images from micro-CT (Figure 3a,f) showed obvious novel bone formation in RADA16, PRG and PDS groups by 4 weeks postoperatively (Figure 3f). The results of quantitative analysis at 2 weeks and at 4 weeks are shown in Figure 3b-e and Figure 3g-I, respectively. At 2 weeks, bone volume fractions (BV/TVs) in the PRG group was significantly greater compared with the Unfilled group ($P < .05$) (Figure 3b). At 4 weeks, PRG and PDS groups showed significantly greater BV/TVs compared with the RADA16 group ($P < .01$ and $P < .05$, respectively) (Figure 3g). There was no difference in the trabecular number in all groups (Figure 3d,i). At 4 weeks, significantly greater values in the trabecular thickness were observed in the RADA16 group ($P < .05$), PRG group ($P < .001$) and PDS group ($P < .001$) compared with the Unfilled group (Figure 3h). The trabecular separation in the PRG and PDS groups were significantly smaller than that in the Unfilled group at 4 weeks ($P < .05$) (Figure 3j). There was no significant difference in BV/TVs, trabecular thickness, number, or separation between PRG and PDS.

3.5 Histological analysis

In all groups, new connective tissue formation was observed in the previous defect area (Figure 4a-d). Often, no inflammatory cell infiltration was observed. At 2 weeks postoperatively, novel bone formation was seen near the root in the defects of the hydrogel groups (Figure 4b-d). Bone formation was very limited in the Unfilled group (Figure 4a). Newly formed bone in the PRG group was significantly greater than that in the Unfilled group (Figure 4a,c). At 4 weeks, formation of new bone in PRG and PDS groups was more pronounced compared to RADA16 group (Figure 4f,g,h). Limited formation of new bone was found in the Unfilled group (Figure 4e).

3.6 Histomorphometric analysis

At 2 weeks postoperatively, epithelial down-growth in the hydrogel groups was reduced compared to the Unfilled group (Figure S4a-d). The epithelial down-growth in PRG and PDS groups at 2 weeks was less than in the Unfilled group (Figure S4a,c,d). There were trends for increase in all groups by 4 weeks (Figure S4e-h). The epithelial down-growth in the RADA16, PRG and PDS groups was smaller than that in the Unfilled group (Figure S4f-h). No obvious difference was found between hydrogel groups (Figure S4c,d,g,h). The results of image analysis were consistent with this observation (Figure S4i,j).

Photomicrographs of samples stained by Azan-Mallory staining are shown in Figure S5a-h. At 2 weeks postoperatively, directions of PDL-like collagen bundles were generally oriented along root surfaces in all groups (Figure S5a-d). No obvious cementum formation was noted. At 4 weeks, in the hydrogel groups, the fiber bundles ran obliquely to the root surface (Figure S5f-h), while they still ran parallel in the Unfilled group (Figure S5e). A thin cementum layer was observed on the root surface in the hydrogel groups (Figure S5f-h). At 4 weeks, mean values for fiber angulation in the RADA16, PRG and PDS groups were significantly greater compared to the Unfilled group ($P < .001$) (Figure S5j).

3.7 Immunohistochemical analyses

Cells positive for PCNA were located in the connective tissue in the Root side (Figure 5a,d), Bone side (Figure 5b,e) and Middle area (Figure 5c,f). At 2 weeks postoperatively, in the Root side, PCNA-positive cells were detected significantly more

in PRG group than in the Unfilled, RADA16, and PDS groups ($P < .01$) (Table 1). In hydrogel groups, the proportions of the positive cells were significantly greater in the Root side and in Middle area than in the Bone side. At 4 weeks, no significant difference was observed between the hydrogel groups in all areas.

VEGF-positive cells were often found close to blood vessels in the connective tissue and around new bone (Figure 6). At 2 weeks, no difference was observed between the hydrogel groups in all area. However, at 4 weeks, in the Middle area, a greater level of VEGF-positive cells was observed in the PRG group than in other groups ($P < .01$) (Table 2).

The results from α-SMA immunohistochemical analysis (Figure S6) showed that, at 2 and 4 weeks postoperatively, the prevalence of α-SMA-positive cells in the Middle area appeared to be pronounced in the PRG group. Quantitative analysis showed that the proportions of α-SMA-positive blood vessels in the PRG group were significantly greater compared to other groups ($P < .01$).

4 Discussion

In this study, we investigated the potentials of RADA16 with two different functional motifs, PRG and PDS, for periodontal regeneration. In our SEM observations, the surface architecture of nanofibers in RADA16 and PDS was similar, but that of PRG was somewhat different. The fiber diameter of PRG was significantly smaller than RADA16 or PDS. It was reported that the number of fibroblasts adhered to nanofibers with PGA/collagen fibers with small diameters was significantly greater than those with large diameters.[38] In SEM analysis, rPDLCs cultured on the PRG showed elongated morphology with pseudopodal projections. It is conceivable that the fiber architecture of PRG is more advantageous for the adherence and ingrowth of native cells.

In vitro, rPDLCs cultured on PRG (RADA16 modified with the RGD motif) showed significantly higher viability/proliferation than PDS or RADA16 at 72 hours. RGD is known to mediate an integrin-receptor type binding with cells. In previous studies, cell non-adhesive, polyvinyl alcohol hydrogels with RGD motif were found to facilitate the attachment and spreading of fibroblasts and osteoblasts.[39,40] Zhang et al.[41] reported that RADA16 with RGD significantly promoted attachment and proliferation of pre-osteoblasts compared to RADA16 alone. Furthermore, it has been shown that human PDL fibroblasts spread well on RADA16 and PRG and migrated deep into PRG.[19] Our CLSM data were consistent with these observations, showing enhanced cell elongation and cell protrusions in the PRG group. Collectively, these results suggest that the designer RADA16 hydrogels, particularly PRG, provide favorable 3-D microenvironment that facilitates cell proliferation.

At 2 weeks postoperatively, BV/TV values were significantly higher in the PRG group compared with the Unfilled group. At 4 weeks, BV/TV values in the PRG and

PDS groups were significantly higher than in the RADA16 group. Trabecular thickness and separation in PRG and PDS groups were significantly different from those in the Unfilled group. It was suggested that bone formation was enhanced in the PRG and PDS groups compared to the Unfilled group. The finding that there was no difference in trabecular thickness, number or separation between the hydrogels suggests that the new bone is still maturing at those time points.

In our previous study using a different periodontal defect model, the application of RADA16 alone lead to a greater bone healing compared to the unfilled control at 4 weeks postoperatively.[17] In the present study, a greater level of bone healing was achieved by using PRG or PDS compared to the RADA16. Kumada & Zhang[19] reported that human PDL fibroblasts proliferated well on PRG compared to RADA16 at 2 weeks, and those cultured on PRG or PDS produced type I and type III collagen by 6 weeks. Human PDL fibroblasts have been reported to adhere to RGD peptide and laminin and express integrin subunits associated with their binding to ECM proteins.[30] Moreover, PRG was shown to enhance the adhesion of human bone marrow mesenchymal stem cells.[22] Considering these and our results of *in vitro* experiments, it was suggested that PRG and PDS increased new bone formation by promoting fibroblast proliferation to greater extent than the RADA16.

In PDL, there are stem cells that could generate cementum and PDL-like tissue.[42] In the current study, PCNA-positive cells were found more in the Root side than in the Bone side in hydrogel groups at 2 weeks postoperatively. It was suggested that most of the cells in the Root side were derived from PDL. In the Root side of connective tissue, PRG application significantly increased the number of PCNA-positive cells compared to other groups. It is possible that PRG allowed effective recruitment of host cells, most

likely from PDL.

VEGF is produced by vascular endothelial cells, chondrocytes, and osteoblasts.[43] VEGF facilitates endothelial cell proliferation, angiogenesis and promotes vascular permeability.[44] Previous studies from our group and others reported that RADA16 could promote angiogenesis and wound healing.[14,17,45] RGD motifs found in ECM structures could play a critical role in angiogenesis.[46] Application of a synthetic hydrogel derived from RGD adhesion motif polyethylene glycol increased traction at the interface between human endothelial cells/gel and promoted angiogenesis.[47] In the present study, VEGF-positive cells were found more in the Root side than in the Bone side in the PRG and PDS groups at 4 weeks postoperatively. This was probably related to the finding that large numbers of PCNA-positive cells and PDLCs were present in the Root side. In the Middle area, increased prevalence of VEGF-positive cells was noted in the PRG group compared with other groups. Furthermore, the results from α-SMA immunohistochemical analysis showed the enhanced prevalence of α-SMA blood vessels in the Middle area in the PRG group. Taken together, it was suggested that PRG fosters cell migration thereby enhancing the expression of VEGF, which, in turn, could lead to angiogenesis.

There are several limitations to this study. Our *in vivo* periodontal defect model does not consider the effect of plaque biofilm. This study focused on the early healing stage using relatively young rats. Determining whether the designer SAP hydrogels enhance total periodontal regeneration requires additional experiments with a longer observation period. Furthermore, clarification of the exact mechanism of the enhanced effects requires studies of molecular and gene levels. Despite the limitations, our findings provide salient insight into the development of more effective scaffolds for periodontal

regeneration.

5 Conclusion

We have shown, for the first time, that local application of the designer SAP hydrogels promoted healing of periodontal defect. Particularly, PRG induced significantly greater cell proliferation of PDL-derived cells *in vitro* and higher expressions of PCNA-, VEGF-, and α-SMA-positive cells *in vivo*, which may have contributed to the enhanced bone healing.

Acknowledgements

We thank Takahiro Takeuchi, DDS, PhD for helpful discussions and Mr. Katsumi Tadokoro for technical guidance.

Conflict of Interest and Source of Funding

There are no conflicts of interest in this study. This work was supported by JSPS KAKENHI (19K19007) and a grant from Multidisciplinary Research Center for Jaw Disease (MRCJD), Tokyo Dental College, Tokyo, Japan (a MEXT Private University Research Branding Project). 3D Matrix (Tokyo, Japan) supplied the SAP hydrogels.

References

1. Narayanan K, Leck KJ, Gao S, Wan AC. Three-dimensional reconstituted extracellular matrix scaffolds for tissue engineering. *Biomater* 2009; 30: 4309-4317.

2. Rios HF, Lin Z, Oh B, Park CH, Giannobile WV. Cell- and gene-based therapeutic strategies for periodontal regenerative medicine. *J Periodontol* 2011; 82: 1223-1237.

3. Hayashi C, Kinoshita A, Oda S, Mizutani K, Shirakata Y, Ishikawa I. Injectable calcium phosphate bone cement provides favorable space and a scaffold for periodontal regeneration in dogs. *J Periodontol* 2006; 77: 940-946.

4. Pérez CMR, Stephanopoulos N, Sur S, Lee SS, Newcomb C, Stupp SI. (2015). The powerful functions of peptide-based bioactive matrices for regenerative medicine. *Annals of Biomedical Engineering* **43**, 501-514.

5. Kao B, Kadomatsu K, Hosaka Y. Construction of synthetic dermis and skin based on a self-assembled peptide hydrogel scaffold. *Tissue Eng Part A* 2009;15: 2385-2396.

6. Zhang S, Holmes TC, DiPersio CM, Hynes RO, Su X, Rich A. Self-complementary oligopeptide matrices support mammalian cell attachment. *Biomater* 1995; 16: 1385-1393.

7. Zhang S. Fabrication of novel biomaterials through molecular self-assembly. *Nat Biotechnol* 2003; 21:1171-1178.

8. Matson JB, Zha RH, Stupp S. Peptide self-assembly for crafting functional biological materials. *Curr Opin Solid State Mater Sci* 2011; 15: 225-235.

9. Semino CE. Self-assembling peptides: from bio-inspired materials to bone regeneration. *J Dent Res* 2008; 87: 606-616.

10. Bradshaw M, Ho D, Fear MW, Gelain F, Wood FM, Iyer KS. Designer self-assembling hydrogel scaffolds can impact skin cell proliferation and migration. *Sci*

Rep 2014; 11: 6903.

11. Miller RE, Grodzinsky AJ, Vanderploeg EJ, et al. Effect of self-assembling peptide, chondrogenic factors, and bone marrow-derived stromal cells on osteochondral repair. *Osteoarthritis and Cartilage* 2010; 18:1608-1619.
12. Markey A, Workman VL, Bruce IA et al. Peptide hydrogel in vitro non-inflammatory potential. *J Pept Sci* 2017; 23: 148-154.
13. Dufour A, Buffier M, Vertu-Ciolino D et al. Combination of bioactive factors and IEIK13 self‐assembling peptide hydrogel promotes cartilage matrix production by human nasal chondrocytes. *J Biomed Mater Res A* 2019; 107: 893-903.
14. Wang R, Wang Z, Guo Y, Li H, Chen Z. Design of a RADA16-based self-assembling peptide nanofiber scaffold for biomedical applications. *J Biomater Sci Polym Ed* 2019; 30: 713-736.
15. Misawa H, Kobayashi N, Soto-Gutierrez A, et al. PuraMatrix facilitates bone regeneration in bone defects of calvaria in mice. *Cell Transplant* 2006; 15: 903-910.
16. Nakahara H, Misawa H, Yoshida A et al. Bone repair using a hybrid scaffold of self‐assembling peptide PuraMatrix and polyetheretherketone cage in rats. *Cell Transplant* 2010; 19: 791-797.
17. Takeuchi T, Bizenjima T, Ishii, Y et al. Enhanced healing of surgical periodontal defects in rats following application of a self-assembling peptide nanofibre hydrogel. *J Clin Periodontol* 2016; 43: 279-288.
18. Linder S, Pinkowski W, Aepfelbacher M. Adhesion, cytoskeletal architecture and activation status of primary human macrophages on a diamond-like carbon coated surface. *Biomater* 2002; 23: 767-773.
19. Kumada Y, Zhang S. Significant type I and type III collagen production from human

periodontal ligament fibroblasts in 3D peptide scaffolds without extra growth factors. *PLoS One* 2010; 22: e10305.

20. Main AL, Harvey TS, Baron M, Boyd J, Campbell ID. The three-dimensional structure of the tenth type III module of fibronectin: an insight into RGD-mediated interactions. *Cell* 1992; 13: 671-678.
21. Durrieu MC, Pallu S, Guillemot F, Bareille R, Amedee J, Baquey CH. Grafting RGD containing peptides onto hydroxyapatite to promote osteoblastic cells adhesion. *J Mater Sci Mater Med* 2004; 15: 779-786.
22. Mota A, Sahebghadam LA, Barzin J, Hatam M, Adibi B, Khalaj Z. Human bone marrow mesenchymal stem cell behaviors on PCL/gelatin nanofibrous scaffolds modified with a collagen IV-derived RGD-containing peptide. *Cell Journal* 2014; 16: 1-10.
23. Pountos I, Panteli M, Lampropoulos A, Jones E, Calori GM, Giannoudis PV. The role of peptides in bone healing and regeneration: a systematic review. *BMC Medicine* 2016; 14: 103.
24. Kim JM, Park WH, Min BM. The PPFLMLLKGSTR motif in globular domain 3 of the human laminin-5 alpha3 chain is crucial for integrin alpha3beta1 binding and cell adhesion. *Exp Cell Res* 2005; 10: 317-327.
25. Terranova VP, Rohrbach DH, Martin GR. Role of laminin in the attachment of PAM 212 (epithelial) cells to basement membrane collagen. *Cell* 1980; 22: 719-726.
26. Murata J, Saiki I, Azuma I, Nishi N. Inhibitory effect of a synthetic polypeptide, poly (Tyr-IIe-Gly-Ser-Arg), on the metastatic formation of malignant tumour cells. *Int J Biol Macromol* 1989; 11: 97-99.
27. Yoon JH, Kim J, Lee H. Laminin peptide YIGSR induces collagen synthesis in Hs27

human dermal fibroblasts. *Biochem Biophys Res Commun* 2012; 23: 416-421.

28. Giannopoulou C, Cimasoni G. Functional characteristics of gingival and periodontal ligament fibroblasts. *J Dent Res* 1996; 75: 895-902.

29. Grzesik WJ, Ivanov B, Robey FA, Southerland J, Yamauchi M. Synthetic integrin-binding peptides promote adhesion and proliferation of human periodontal ligament cells in vitro. *J Dent Res* 1988; 77: 1606-1612.

30. Palaiologou AA, Yukna RA, Moses R, Lallier TE. Gingival, dermal, and periodontal ligament fibroblasts express different extracellular matrix receptors. *J Periodontol* 2001; 72: 798-807.

31. Maude S, Ingham E, Aggeli A. Biomimetic self-assembling peptides as scaffolds for soft tissue engineering. *Nanomedicine* 2013; 8: 823-847.

32. Horii A, Wang XM, Gelain F, Zhang S. Biological designer self assembling peptide nanofiber scaffolds significantly enhance osteoblast proliferation, differentiation and 3-D migration. *PloS ONE* 2007; 2: e190.

33. Inoue T, Deporter DA, Melcher AH. Induction of chondrogenesis in muscle, skin, bone marrow, and periodontal ligament by demineralized dentin and bone matrix in vivo and in vitro. *J Dent Res*1986; 65: 12-22.

34. Yoshida W, Matsugami D, Murakami T, et al. Combined effects of systemic parathyroid hormone (1-34) and locally delivered neutral self-assembling peptide hydrogel in the treatment of periodontal defects: An experimental in vivo investigation. *J Clin Periodontol* 2019; 46: 1030-1040.

35. Bizenjima T, Seshima F, Ishizuka Y, Takeuchi T, Kinumatsu T, Saito A. Fibroblast growth factor-2 promotes healing of surgically created periodontal defects in rats with early, streptozotocin-induced diabetes via increasing cell proliferation and

regulating angiogenesis. *J Clin Periodontol* 2015; 42: 62–71.

36. Park CH, Rios HF, Jin Q, et al. Tissue engineering bone-ligament complexes using fiber-guiding scaffolds. *Biomater* 2012; 33: 137–145.

37. Lucarini G, Zizzi A, Aspriello SD, et al. Involvement of vascular endothelial growth factor, CD44 and CD133 in periodontal disease and diabetes: an immunohistochemical study. *J Clin Periodontol* 2009; 36: 3–10.

38. Tian F, Hosseinkhani H, Hosseinkhani M, et al. Quantitative analysis of cell adhesion on aligned micro- and nanofibers. *J Biomed Mater Res A* 2008; 84: 291–299.

39. Burdick JA, Anseth KS. Photoencapsulation of osteoblasts in injectable RGD-modified PEG hydrogels for bone tissue engineering. *Biomater* 2002; 23: 4315–4323.

40. Schmedlen RH, Masters KS, West JL. Photocrosslinkable polyvinyl alcohol hydrogels that can be modified with cell adhesion peptides for use in tissue engineering. *Biomater* 2002; 23: 4325–4332.

41. Zhang F, Shi GS, Ren LF, Hu FQ, Li SL, Xie ZJ. Designer self-assembling peptide scaffold stimulates pre-osteoblast attachment, spreading and proliferation. *J Mater Sci Mater Med* 2009; 20: 1475-1481.

42. Seo BM, Miura M, Gronthos S, et al. Investigation of multipotent postnatal stem cells from human periodontal ligament. *Lancet* 2004; 364: 149-155.

43. Harada S, Nagy JA, Sullivan KA, et al. Induction of vascular endothelial growth factor expression by prostaglandin E2 and E1 in osteoblasts. *J Clin Invest* 1994; 93: 2490-2496.

44. Unlü F, Güneri PG, Hekimgil M, Yeşilbek B, Boyacioğlu H. Expression of vascular endothelial growth factor in human periodontal tissues: comparison of healthy and diabetic patients. *J Periodontol* 2003; 74: 181-187.

45. Meng H, Chen L, Ye Z, Wang S, Zhao X. The effect of a self-assembling peptide nanofiber scaffold (peptide) when used as a wound dressing for the treatment of deep second degree burns in rats. *J Biomed Mater Res B Appl Biomater* 2009; 89: 379-391.

46. Yu J, Du KT, Fang Q, et al. The use of human mesenchymal stem cells encapsulated in RGD modified alginate microspheres in the repair of myocardial infarction in the rat. *Biomater* 2010; 31: 7012-7020.

47. Zisch AH, Lutolf MP, Ehrbar M, et al. Cell-demanded release of VEGF from synthetic, biointeractive cell ingrowth matrices for vascularized tissue growth. *FASEB J* 2003; 17: 2260-2262.

TABLE 1 Quantitative analysis of PCNA-positive cells

Group	Unfilled	RADA16	PRG	PDS
2 weeks				
Root side	20.3 ± 4.5	42.6 ± 6.2[a,*]	56.1 ± 4.0[a,b,c,*]	48.0 ± 2.7[a,*]
Bone side	21.0 ± 3.7	31.4 ± 6.0[a]	34.4 ± 3.2[a]	32.1 ± 5.0[a]
Middle area	18.1 ± 3.1	44.5 ± 4.4[a,*]	52.0 ± 6.0[a,*]	46.3 ± 7.6[a,*]
4 weeks				
Root side	17.9 ± 5.2	32.9 ± 5.5[a]	38.8 ± 4.5[a]	40.0 ± 5.3[a]
Bone side	19.4 ± 3.7	30.1 ± 7.7[a]	32.9 ± 4.3[a]	36.1 ± 6.1[a]
Middle area	19.9 ± 4.6	30.4 ± 6.4[a]	38.0 ± 5.6[a]	34.8 ± 6.0[a]

Data shown as mean ± SD (n=8) of PCNA-positive cells / total cells (%) in the count area (Root side, Bone side, Middle area). PCNA, Proliferating cell nuclear antigen.

a; significantly different from the Unfilled group, b; from the RADA16 group, c; from the PDS group, *; significantly different from the Bone side, by ANOVA with Tukey post hoc test ($P < .05$ - $.0001$).

TABLE 2 Quantitative analysis of VEGF-positive cells

Group	Unfilled	RADA16	PRG	PDS
2 weeks				
Root side	4.8 ± 1.6	8.7 ± 2.1[a]	8.8 ± 1.9[a]	7.8 ± 1.7[a]
Bone side	5.0 ± 1.6	7.3 ± 1.5	8.8 ± 2.0[a]	8.0 ± 1.4[a]
Middle area	5.3 ± 1.9	9.4 ± 2.2[a]	12.1 ± 2.6[a,*]	11.0 ± 1.6[a,*,**]
4 weeks				
Root side	8.0 ± 2.1	12.4 ± 2.4[a]	18.8 ± 2.6[a,b,**]	15.1 ± 3.4[a,**]
Bone side	7.8 ± 2.1	11.2 ± 2.6[a]	13.1 ± 1.6[a]	11.0 ± 1.5
Middle area	8.0 ± 1.7	12.1 ± 2.6[a]	18.3 ± 2.6[a,b,c,**]	12.3 ± 2.8[a]

Data shown as mean ± SD (n = 6) of VEGF-positive cells / total cells (%) in the count area (Root side, Bone side, Middle area). VEGF, vascular endothelial growth factor.

a; significantly different from the Unfilled group, b; from the RADA16 group, c; from the PDS group, *; significantly different from the Root side, **; from the Bone side, by ANOVA with Tukey post hoc test ($P < .05$ - $.0001$).

Figure legends

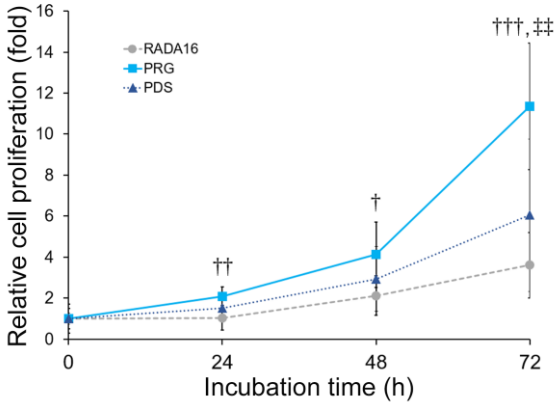

FIGURE 1 Viability/proliferation of rat periodontal ligament-derived cells (rPDLCs). rPDLCs were cultured on the RADA16, PRG or PDS with medium or medium alone (control). WST-1 assay was used to assess cell viability/proliferation at indicated time points. In each group, values relative to those at 0 h were shown. Data presented as mean ± SD (n = 7). $^{\dagger}P < .05$, $^{\dagger\dagger}P < .01$, $^{\dagger\dagger\dagger}P < .001$ compared with the RADA16 group, and $^{\ddagger\ddagger}P < .01$ compared with the PDS group, by ANOVA with Tukey post hoc test

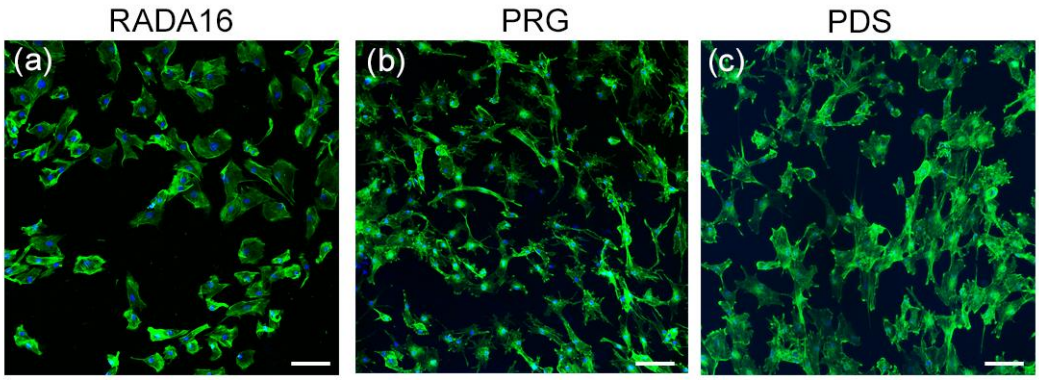

FIGURE 2 Representative confocal laser scanning microscopy images.
At 72 hours, cells on PRG or PDS appear to be elongated and show cell protrusions. (Green; actin cytoskeleton). (original magnification ×100, bar = 100 μm)

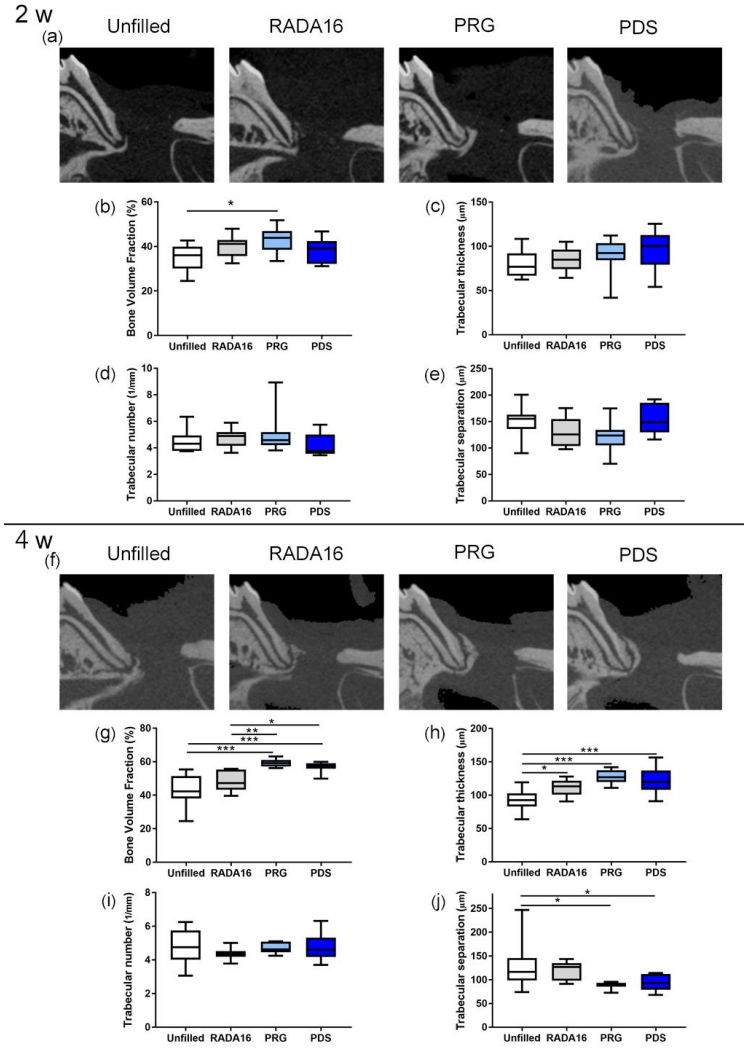

FIGURE 3 Two-dimensional micro-CT images and quantification results.

(a,f) A sagittal slice images from micro-CT. Marked bone formation is observed in PRG and PDS groups at 4 weeks postoperatively. (b-e, g-j) Quantification of micro-CT images using TRI/3D-BON. White bar, Unfilled group; Gray bar, RADA16 group; Light blue bar, PRG group; Blue bar, PDS group. The BV/TVs (b,g), Trabecular thickness (c, h), Trabecular number (d, i), and Trabecular separation (e,j) were compared between groups. Data presented as box-and-whiskers plots showing minimum, maximum, median and 25th and 75th percentiles (n = 10). **P* < .05, ***P* < .01, ****P* < .001 by ANOVA with Tukey post-test

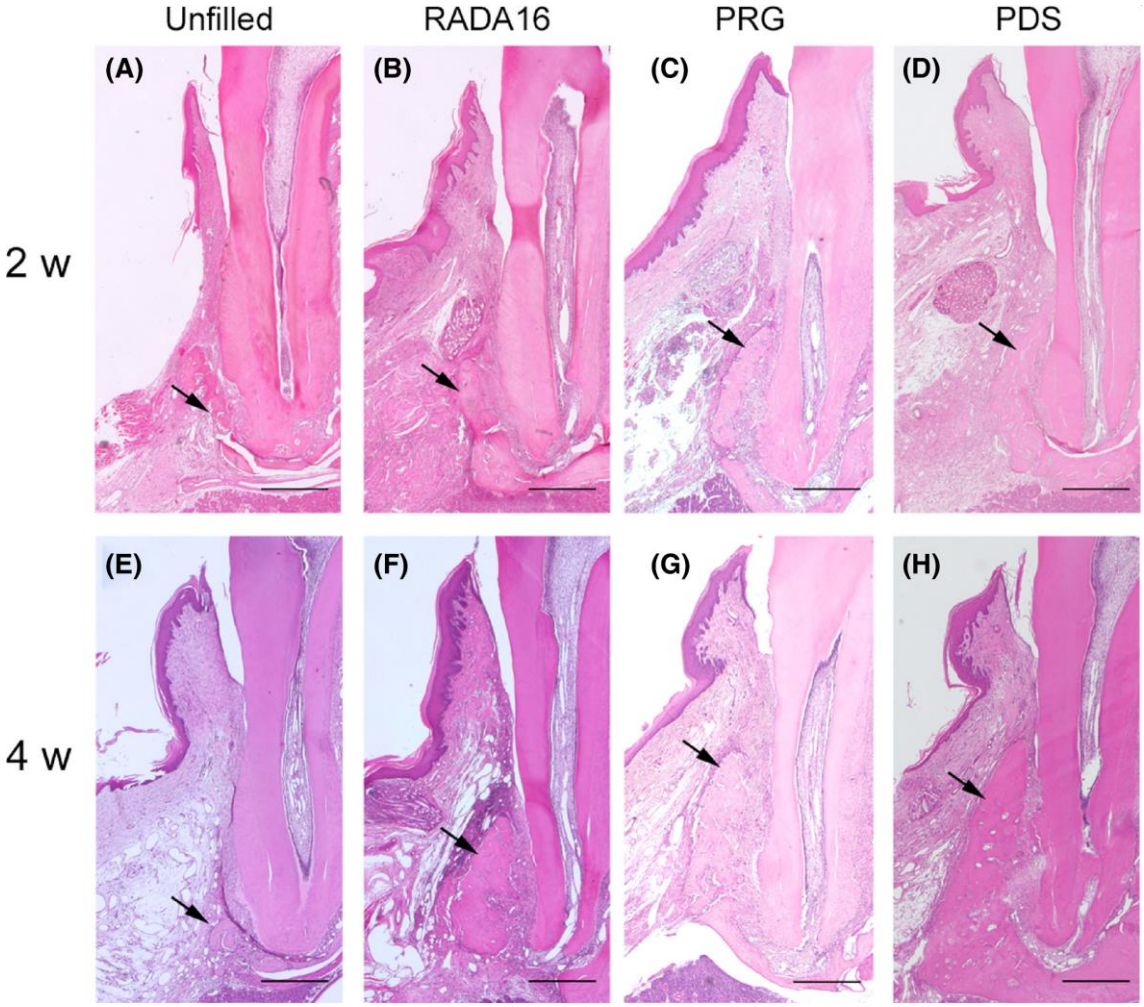

FIGURE 4 Histopathological analysis (H&E staining).

At 2 weeks postoperatively, connective tissue filled the previous defect area. (a) Formation of new bone is not observed in the Unfilled group. (b-d) In RADA16, PRG and PDS groups, novel bone formation from the tooth side is observed.

(e) At 4 weeks, bone formation is limited in the Unfilled group. (h) The level of new bone in the hydrogel groups appears to be greater than Unfilled group. Arrows indicate new bone. (original magnification ×25, bar = 500 μm)

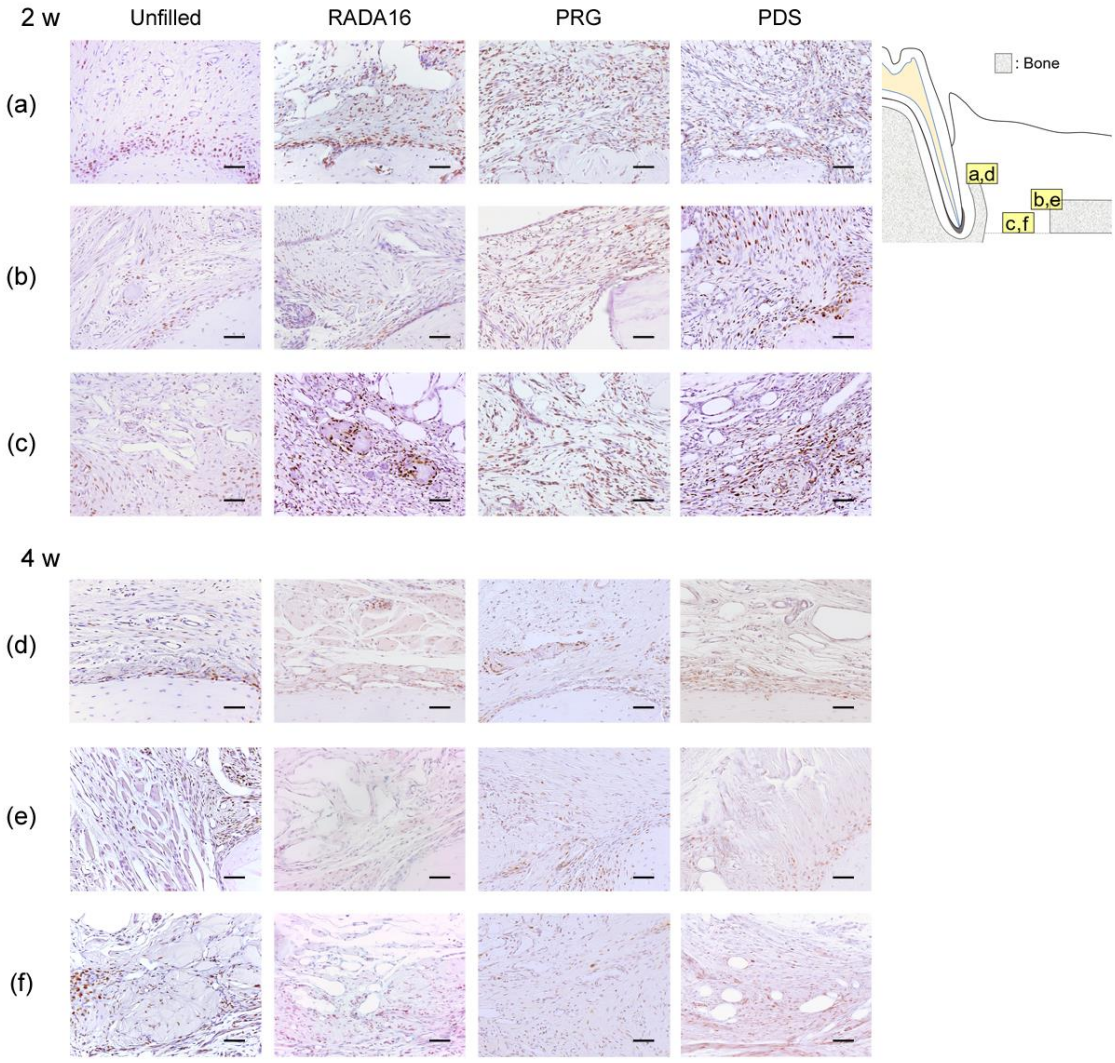

FIGURE 5 Representative images of PCNA staining.

Prevalence of PCNA-positive cells was assessed in Root side (a,d), Bone side (b,e), and middle area (c,f). PCNA-positive cells are shown as brown staining. At 2 weeks postoperatively, the number of PCNA-positive cells in Root side (a) are greater in the PRG group compared to other groups. At 4 weeks, no obvious difference in the prevalence of PCNA-positive cells between groups is observed in any of the areas (d–f). (original magnification ×200; bar = 50 μm)

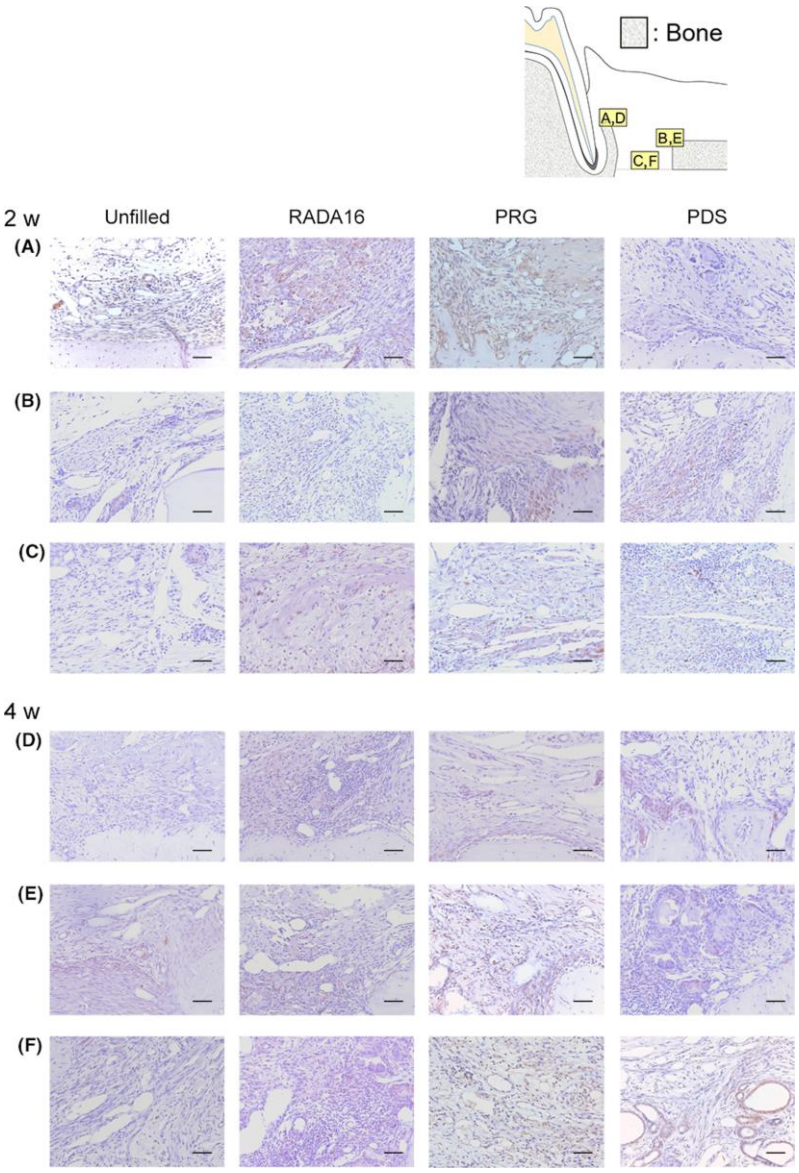

FIGURE 6 Representative images of VEGF immunohistochemical analysis. Prevalence of VEGF-positive cells were assessed in Root side (a,d), Bone side (b,e), and Middle area (c,f). VEGF-positive reaction appears brown. At 2 and 4 weeks postoperatively, the prevalence of VEGF-positive cells in hydrogel groups appears to be greater than in the Unfilled group (a-e). At 4 weeks, more VEGF-positive cells can be observed in the PRG group (f) compared with other groups.
(original magnification ×200; bar = 50 μm)

Supplemental files

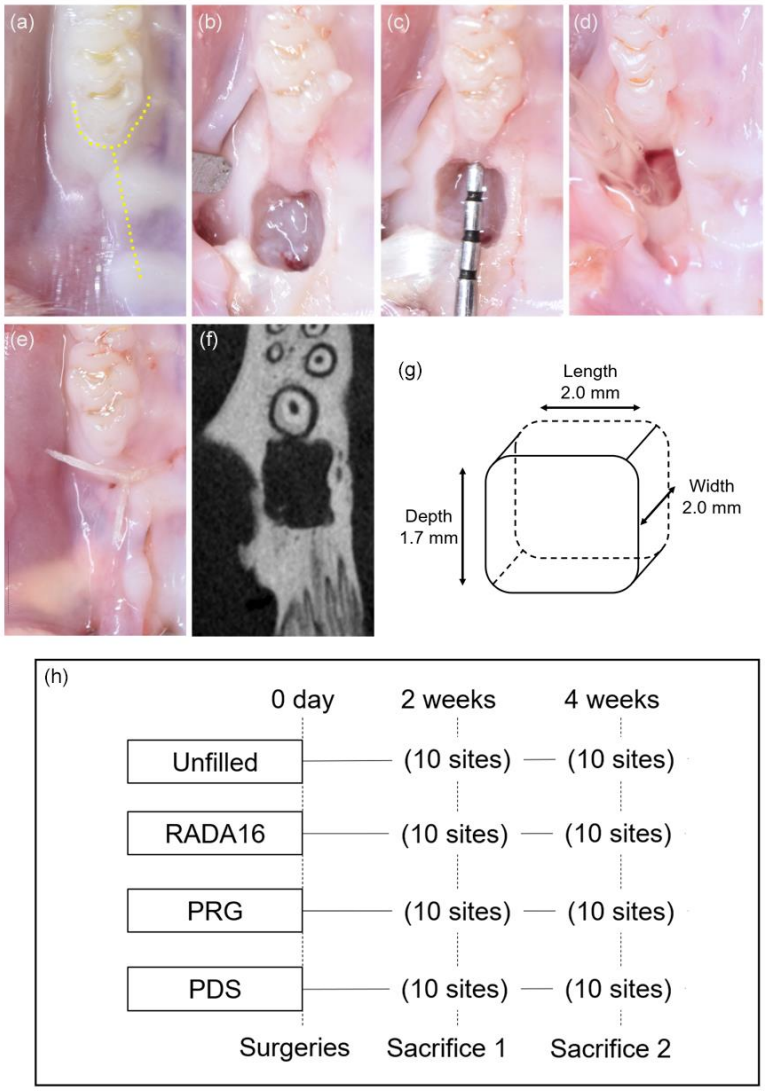

FIGURE S1 Periodontal defect creation and the protocol for *in vivo* experiments. (a) Incision design (b) After raising full-thickness flaps, bilateral standardized periodontal defects were created at the mesial aspect of the maxillary first molars. (c) Confirmation of the defect size. A surgical template was used to create each defect (2.0×2.0×1.7 mm). (d) Application of RADA16, PRG or PDS (2.5%). (e) Resorbable sutures were used to close the flaps. (f) Micro-CT image of periodontal defect. (g) Defect size. (h) *In vivo* protocol and grouping.

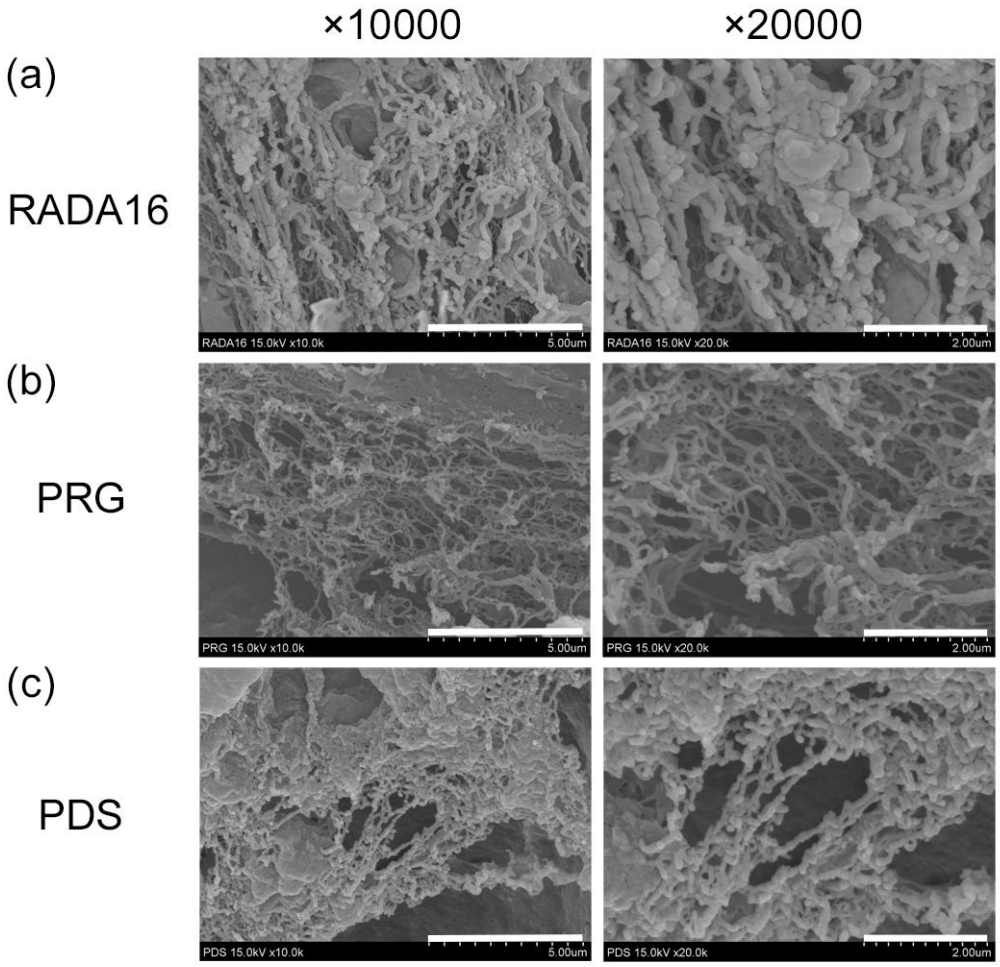

FIGURE S2 SEM analysis of the SAP hydrogels used.

(a) RADA16, (b) PRG and (c) PDS, showing fibrous structure with nanopores (range 5–200 nm). The mesh fiber surfaces of RADA16 and PDS appear to be coarse. On the other hand, that of PRG is smoother and the fiber is finer. (original magnification × 10000, bar = 5 μm, and original magnification × 20000, bar = 2 μm)

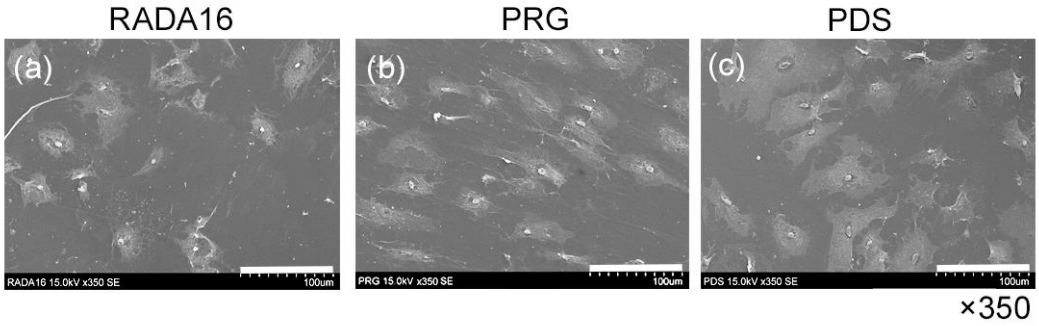

FIGURE S3 SEM analysis of rPDLCs cultured on the hydrogels.

(a) RADA16, (b) PRG and (c) PDS. At 72 hours, rPDLCs on RADA16 appear roundish. In contrast, the cells on hydrogels, especially PRG, appear elongated with pseudopodal projections. (original magnification × 350, bar = 100 μm)

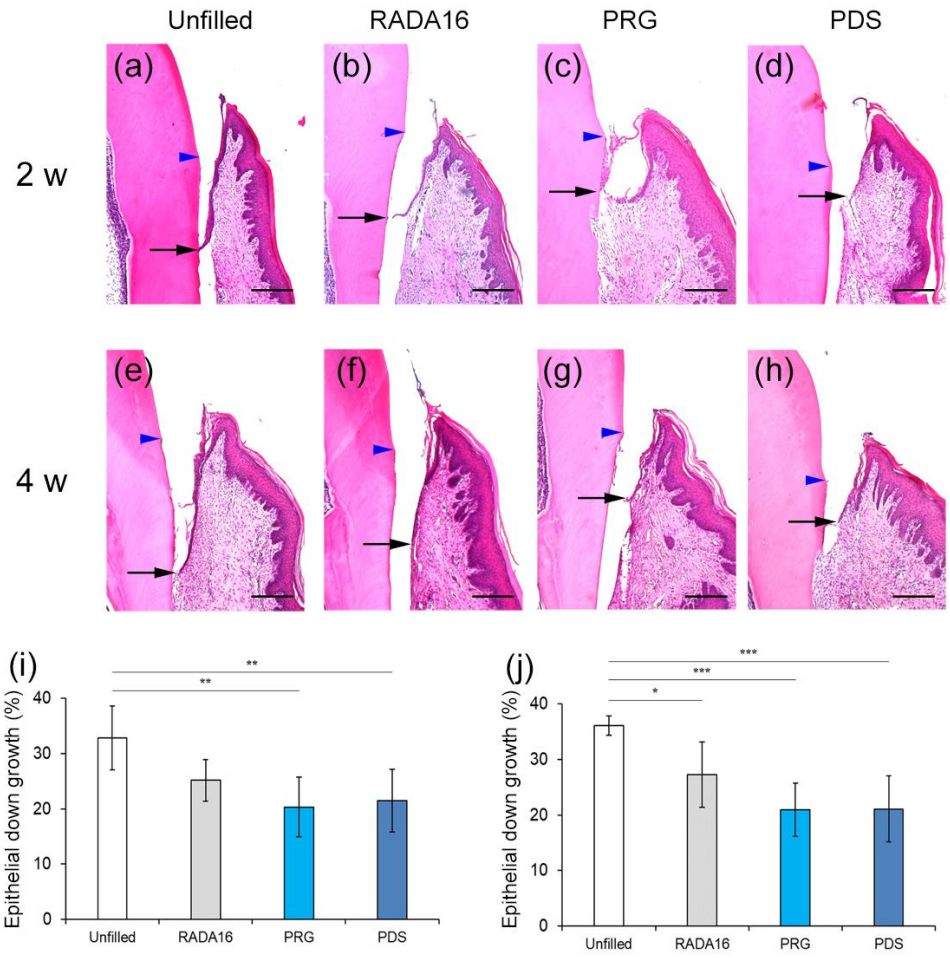

FIGURE S4 Histomorphometric assessment of epithelial down-growth.

(a-d and e-h) Black arrows indicate the apical extent of the epithelial attachment. Blue arrowheads indicate CEJ. (a-d) Epithelial down-growth in RADA16, PRG and PDS groups appears to be reduced compared to the Unfilled group at 2 weeks postoperatively. (e-h) A trend for progression of down-growth can be observed at 4 weeks (original magnification ×50; bar = 200 μm).

(i, j) Quantitative assessment of epithelial down-growth. Data presented as mean ± SD (n=6) of (the length between the most coronal and most apical extents of the junctional epithelium) / (the distance between CEJ and the defect base) (%) at 2 and 4 weeks postoperatively. *P < .05, **P < .01, ***P < .001 by ANOVA with Tukey post-test.

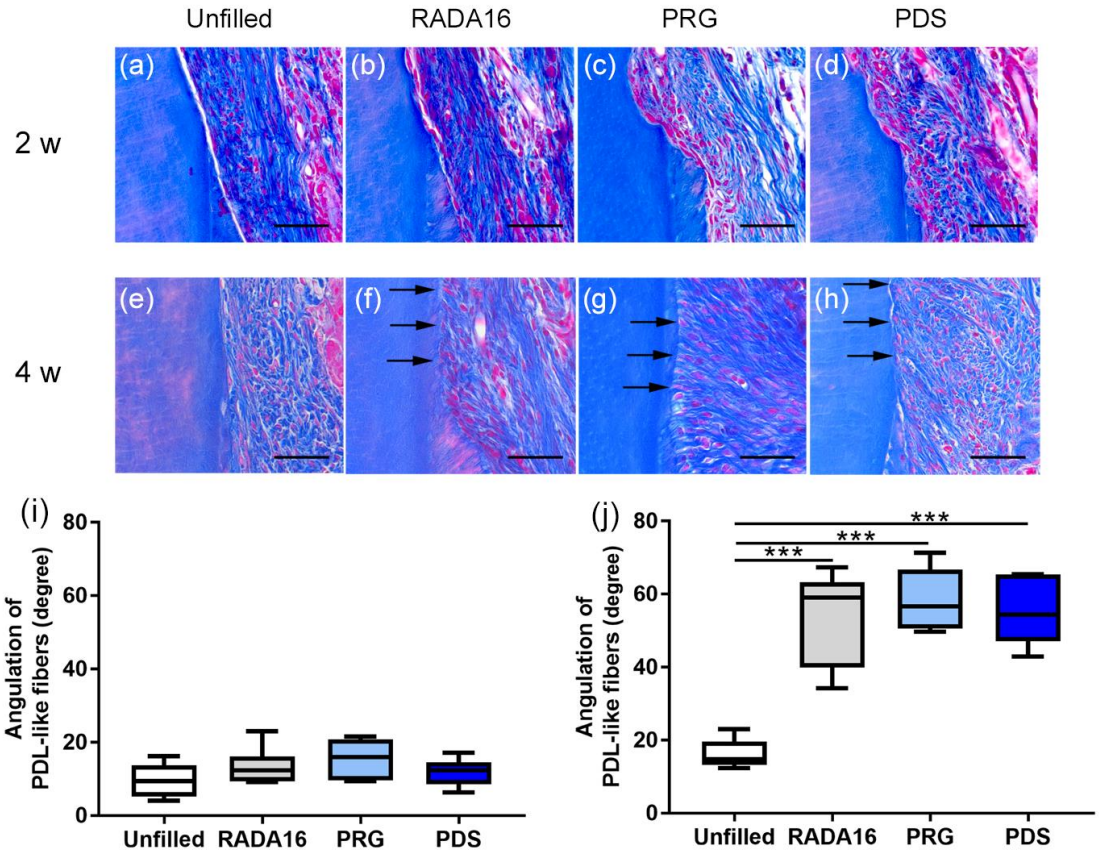

FIGURE S5 Healing of periodontal ligament (PDL).

(a-h) Representative images of the root region near the defect base. (a-d) At 2 weeks postoperatively (upper panel), PDL-like fiber bundles are observed along the root surface in all groups. (f, g, h) At 4 weeks, fiber bundles run obliquely and are inserted into the root surface with thin cementum layer (arrow). (e) In other groups, fiber bundles appear along the root surfaces. (Azan–Mallory's stain, original magnification ×200; bar = 50 μm). (I, J) Angulation of the PDL-like fibers. Fiber angle was assessed by Image J at 2 weeks (i) and 4 weeks (j) postoperatively. Data shown as box-and-whiskers plots showing minimum, maximum, median and 25th and 75th percentiles (n=6) in degree. ***$P < .001$ by ANOVA with Tukey post-test.

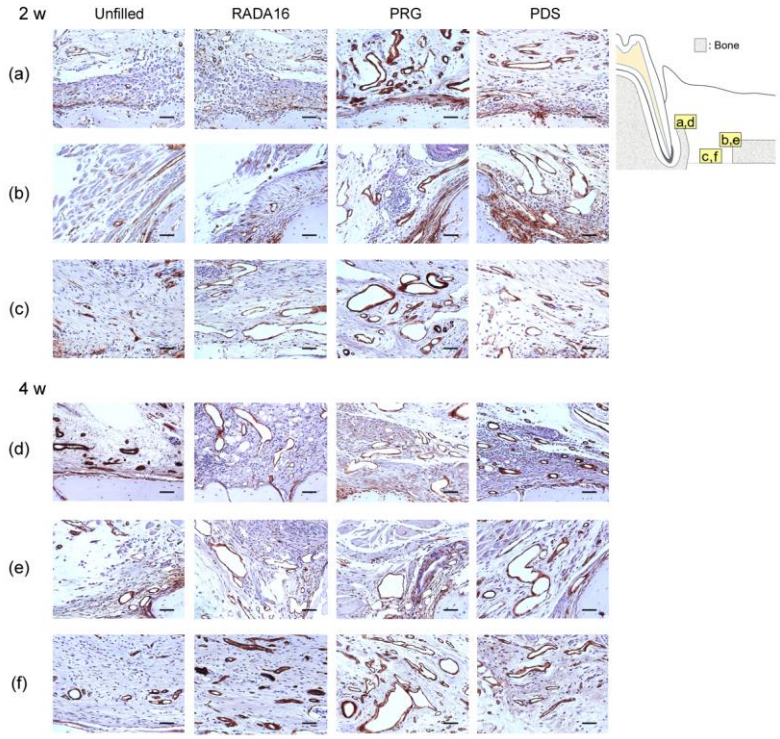

TABLE Quantitative analysis of α-SMA -positive blood vessels

Group	Unfilled	RADA16	PRG	PDS
2 weeks				
Root side	9.6 ± 4.0	13.2 ± 3.4	22.0 ± 3.1[a,b]	16.8 ± 5.8
Bone side	8.4 ± 1.5	11.2 ± 5.0	12.4 ± 1.8	12.6 ± 5.2
Middle area	7.2 ± 2.9	14.0 ± 2.3[a]	28.8 ± 5.8[a,b,c]	17.0 ± 2.9[a]
4 weeks				
Root side	12.2 ± 3.3	16.2 ± 2.2	27.4 ± 8.2[a,b]	27.0 ± 4.1[a,b]
Bone side	14.0 ± 3.0	16.6 ± 2.5[a]	18.4 ± 5.8[a]	16.4 ± 7.2
Middle area	14.8 ± 4.5	27.0 ± 3.8[a]	40.2 ± 5.0[a,b,c]	27.8 ± 4.0[a]

Data shown as mean ± SD (n = 5) of α-SMA -positive blood vessels in the count area (Root side, Bone side, Middle area). α-SMA, α-smooth muscle actin.
a; significantly different from the Unfilled group, b; from the RADA16 group, c; from the PDS group, by ANOVA with Tukey post hoc test ($P < .05$ - $.001$).

FIGURE S6 Representative photomicrographs of immunohisotochemical staining for α-SMA and quantitative data. Prevalence of α-SMA-positive cells were assessed in Root side (a,d), Bone side (b,e), and Middle area (c,f). α-SMA-positive reaction appears brown. At 2 and 4 weeks postoperatively, in the Middle area, the prevalence of α-SMA-positive blood vessels is more pronounced in the PRG group. (original magnification ×200; bar = 50 μm). Quantitative analysis showed that the proportions of α-SMA blood vessels in the PRG group were significantly greater compared to other groups.